Peeling under large bending deformations

Follower versus fixed loads. A unified approach for concentrated or distributed loads

Barbieri, Ettore; Botto, Lorenzo

DOI
10.1016/j.ijsolstr.2022.111450

Publication date
2022

Document Version
Final published version

Published in
International Journal of Solids and Structures

International Journal of Solids and Structures 241 (2022) 111450

Contents lists available at ScienceDirect

International Journal of Solids and Structures

journal homepage: www.elsevier.com/locate/ijsolstr

Peeling under large bending deformations: Follower versus fixed loads. A unified approach for concentrated or distributed loads

Ettore Barbieri [a,*], Lorenzo Botto [b]

[a] Japan Agency for Marine-Earth Science and Technology (JAMSTEC)
Research Institute for Value-Added Information Generation (VAiG)
Center for Mathematical Science and Advanced Technology (MAT)
, Yokohama Institute for Earth Sciences (YES), 3173-25, Showa-machi, Kanazawa-ku, Yokohama-city, Kanagawa, 236-0001, Japan
[b] Delft University of Technology, Department of Process & Energy, Mekelweg 2 2628 CD Delft, Netherlands

ARTICLE INFO

Keywords:
Follower
Strain energy release rate
Peeling
Hydrodynamic
Graphene

ABSTRACT

In the non-dissipative regime, the potential energy is the difference between the strain energy of the deforming solid and the work done by the external forces. For configuration-dependent external forces, whose direction is perpendicular to the deformed shape, we obtain a simple formula for the strain energy release rate of peeled strips experiencing large deformations and prove rigorously that the same formula applies for external forces having fixed direction.

We then apply Griffith's criterion for fracture to calculate critical loads for two cases: peeling produced by a uniform follower pressure distributed along the flexible strip and peeling produced by a localized follower shear force applied at the edge of the strip.

We found that for these loads, the critical pressure for peeling follows approximately $q_c \sim \Gamma L^{-1}$, where Γ is the solid–solid interface energy and L is the initial peeling length; for the shear force, the corresponding critical value instead follows $Q_{0_c} \sim \Gamma$, independently of the initial length.

These formulas are, unexpectedly, independent of the bending stiffness EI of the strips and differ from the ones predicted for small deformations, i.e. $q_c \propto L^{-2}\sqrt{EI\,\Gamma}$ and $Q_{0_c} \propto L^{-1}\sqrt{EI\,\Gamma}$.

We apply our results to predict the critical hydrodynamic load necessary to exfoliate graphene sheets from graphite, a fluid–structure interaction problem where the load is of the follower type. We find that a follower load peeling model gives significantly improved predictions than fixed load peeling. For the same Γ, L and b, the critical hydrodynamic follower load is always lower than the one with fixed forces: approximately half for the case with uniform pressure, and one third for the case with shear force.

1. Introduction

In fluid–structure interaction problems with small structural deformations, one can assume that the flow-induced load has a fixed direction. Instead, for large structural deformations, the flow-induced force "follows" the structure (Mandre and Mahadevan, 2009; Pigolotti et al., 2017; Bayly and Dutcher, 2016; Aoi et al., 2013; De Canio et al., 2017; Gravelle et al., 2020). This case is known in the literature as "follower load" (Wood et al., 1969; Sugiyama et al., 1995, 1999, 2000).

Calculating the external work done by a follower load to predict the emergence of fracture is not an easy task, and because of this, many theoretical papers assume a fixed load. However, for flexible structures, this assumption can lead to erroneous predictions (Zehnder and Potdar, 1998; Anderson, 1991). Such a situation arises in peeling problems where the ratio of bending to hydrodynamic forces is small. For example, in liquid-phase exfoliation of graphite to make graphene, the hydrodynamic load due to the fluid breaks the van der Waals adhesive bonds between graphene layers (Salussolia et al., 2020; Botto, 2019). The bending rigidity of graphene layers is minimal, causing large deformations of the layers. Besides liquid-phase exfoliation, such a problem is also encountered in applications to hydraulic fracturing (Lenoach, 1995), flow-accelerated corrosion by flaking (Medvedovski et al., 2020), blood cell adhesion in flowing conditions (Hodges and Jensen, 2002), removal of adhesives and others.

In the quasi-static limit, Griffith's theory states that the critical load to peel off a flexible layer derives from a balance between the rates of change of the system's potential energy, as the peeling front extends the corresponding change in surface energy. The potential energy of

* Corresponding author.
E-mail address: e.barbieri@jamstec.go.jp (E. Barbieri).

https://doi.org/10.1016/j.ijsolstr.2022.111450
Received 13 August 2021; Received in revised form 13 January 2022; Accepted 18 January 2022
Available online 14 February 2022

the peeled layer is

$$\Pi = U - W, \tag{1}$$

where U is the strain energy stored in the deformation and W is the work done by the external forces. If we consider a thin sheet of width b and peeled length L (Fig. 1(a)), Griffith's energy balance reads

$$G = -\frac{1}{b}\frac{\partial \Pi}{\partial L} = \Gamma, \tag{2}$$

where Γ is the surface energy per unit area. If an expression for Π as a function of the load is available, Griffith's condition (2) can be used to find the critical load beyond which the peeling front will extend. This paper analyzes theoretically and numerically how to calculate W (and therefore G) for follower loads applied either at the edge (see Fig. 1(a)) or distributed uniformly on the deforming structure.

For follower loads, the application of Griffith's criterion poses two issues. Firstly, configuration-dependent forces are not derivable from a potential (Antman, 1995; Berry and Shukla, 2015, 2016). Secondly, the large deformations typical of follower loads prevent the use of Clapeyron's theorem, which states that $W = 2U$. For large deformations, the connection between W and U is unclear. Despite the rich literature on the stability of structures loaded by non-conservative forces (Bigoni and Noselli, 2011; Bigoni et al., 2018b,a; Bigoni and Misseroni, 2020; Kirillov, 2013; Tommasini et al., 2016), we are aware of only one work addressing the calculation of the external work with follower forces. Libai and Simmonds (1988) provided the following expression for the *apparent external mechanical power* $\dot{W}$ of a rod loaded by a hydrostatic pressure per unit width q and a concentrated force per unit width $\mathbf{F}$

$$\dot{W} = \mathbf{F}\cdot\mathbf{v} + q\int_0^L \left(x'\,\dot{y} - y'\,\dot{x}\right)\,\mathrm{d}S, \tag{3}$$

where $(\cdot)' = \mathrm{d}/\mathrm{d}S$, with S being the arc length, x and y the deformation of the rod and $\mathbf{v} = \dot{\mathbf{x}} = (\dot{x}, \dot{y})$. Although correct, this equation does not provide insights into the connection between the external work and the strain energy, which is instead explicitly provided by Clapeyron's theorem for small deformations.

In this paper we carry out a detailed mathematical analysis of the external work in peeling caused by a follower load of constant magnitude and direction depending on the normal to the deformable structure. Although follower forces are not conservative, they are not dissipative. We use this feature to arrive at a general integral expression involving the strain energy. We consider the case of a shear follower load applied at the edge, of constant magnitude Q_0 (Section 3.1) and the case of a uniform distributed force (per unit length) q along the length of a peeled structure (Section 3.2). This second case is referred to as pressure load. We also verify our approach by applying it to the case of Kendall's peeling (Kendall, 1971, 1975) (Section 3.3). The expressions for G in the two cases are analyzed in Section 4. In Section 5 we compare critical loads obtained with our expressions for large follower deformations with the critical loads assuming small deformations and applied loads of constant direction.

2. Equilibrium equations

The equations of equilibrium of forces and moments of an inextensible elastic rod are (Frisch-Fay, 1962; Antman, 1968):

$$\begin{aligned} &Q' - \mu N - q = 0,\\ &N' + \mu Q = 0,\\ &M' - Q = 0, \end{aligned} \tag{4}$$

where $(\cdot)' = \mathrm{d}/\mathrm{d}S$ with S being the arc length, Q is the shear force, μ is the curvature, N is the axial force, M is the bending moment and q is a distributed normal load (Fig. 1(b)). In writing Eq. (4) we neglected the shear strains. In addition, we are considering quasi-static conditions. Experimentally, such situations are tricky to reproduce and the system becomes unstable for large loads (Misseroni et al., 2021). The shape of the elastica can be found by solving

$$\begin{aligned} &\theta' = \mu,\\ &x' = \cos\theta,\\ &y' = \sin\theta, \end{aligned} \tag{5}$$

where θ is the rotation, $x(S)$ and $y(S)$ are the Cartesian coordinates of a point of the rod and assuming a linear elastic constitutive model

$$M = E\,I\,\mu, \tag{6}$$

with E the Young modulus and I the (second) moment of area of the cross-section, which is assumed constant. We introduce the following dimensionless variables:

$$S^* = \frac{S}{L}, \qquad \mu^* = \mu\,L, \tag{7}$$

with L being the length of the rod. We obtain the following dimensionless parameters appearing in the boundary conditions:

$$M_0^* = \frac{M_0\,L}{E\,I}, \qquad Q_0^* = \frac{Q_0\,L^2}{E\,I}, \qquad N_0^* = \frac{N_0\,L^2}{E\,I}, \qquad q^* = \frac{q\,L^3}{E\,I}, \tag{8}$$

with M_0 being a moment applied to the free end, Q_0 a terminal shear force, N_0 an applied terminal axial force and q a distributed load, where $(\cdot)_0$ refers to variables at $S = 0$. The system of Eqs. (4) can be combined in the single equation

$$\mu'' + \frac{1}{2}\mu^3 - A\,\mu - q = 0, \tag{9}$$

with

$$A = N_0 + \frac{1}{2}{\mu_0}^2. \tag{10}$$

We have removed the $(\cdot)^*$ for ease of reading. Multiplying both sides of Eq. (9) by μ' and assuming q to be *uniform*, integrating between 0 and S yields

$${\mu'}^2 + \frac{\mu^4}{4} - A\,\mu^2 - 2\,q\,\mu = B, \tag{11}$$

where

$$B = {N_0}^2 + {Q_0}^2 - A^2 - 2\,\mu_0\,q. \tag{12}$$

Eq. (11) includes all possible combinations of boundary conditions. We will consider three separate cases. Case 1 assumes a shear follower force applied at the end, but no distributed load:

$$Q_0 > 0 \qquad q = 0 \qquad N_0 = 0 \qquad \mu_0 = 0$$

$${\mu'}^2 + \frac{\mu^4}{4} = {Q_0}^2, \tag{13a}$$

$$\mu(0) = 0. \tag{13b}$$

Case 2 considers a distributed uniform load, but no shear force:

$$Q_0 = 0 \qquad q > 0 \qquad N_0 = 0 \qquad \mu_0 = 0$$

$${\mu'}^2 + \frac{\mu^4}{4} - 2\,q\,\mu = 0, \tag{14a}$$

$$\mu(0) = 0. \tag{14b}$$

Case 3 analyzes an applied axial force and moment at the free end, which represents the Kendall peeling (Kendall, 1975).

$$Q_0 = 0 \qquad q = 0 \qquad N_0 > 0 \qquad \mu_0 > 0$$

$${\mu'}^2 = \frac{1}{4}\left(\mu^2 - {\mu_0}^2\right)\left({\mu_0}^2 + 4\,N_0 - \mu^2\right) \tag{15a}$$

$$\mu(0) = \mu_0. \tag{15b}$$

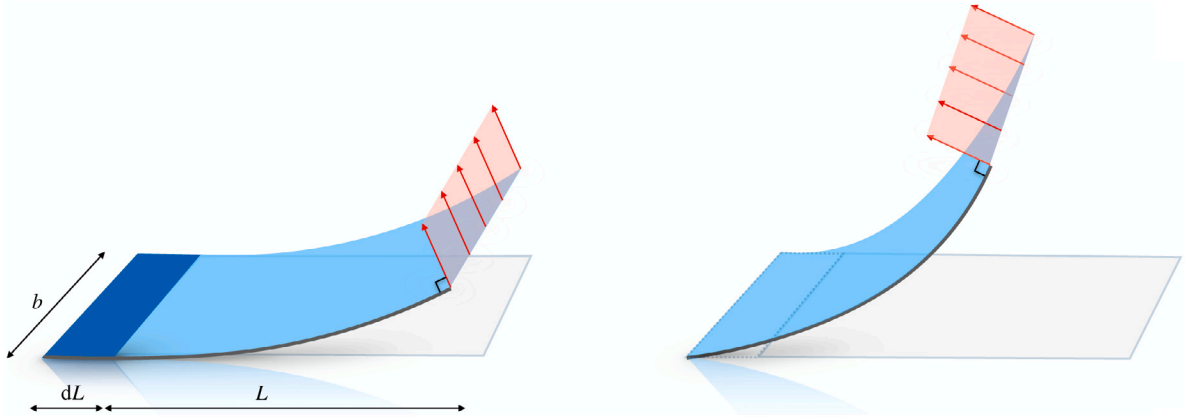

(a) Peeling by a terminal shear force

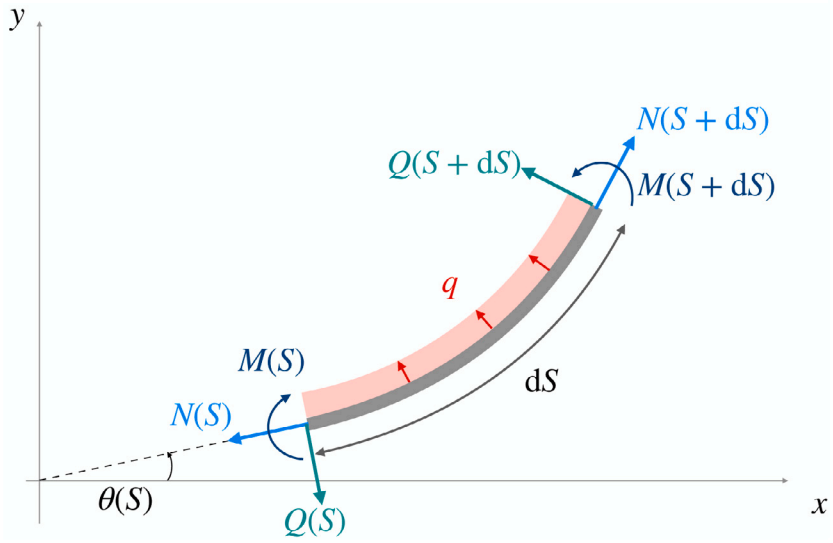

(b) Free body diagram

Fig. 1. Description of the problem and free body diagram.

3. Analysis of the external work

We now focus on the key contribution of this paper, which is the calculation of the external work. We assume load-controlled and quasi-static conditions.

Firstly, we will illustrate with a simple example the rationale behind our approach. Let us consider a spring system, with stiffness k, subjected to a force Q_0. The displacement of the spring from the equilibrium position is $u = Q_0/k$. The work done by the force is the area of the rectangle with diagonal $(0,0)$ and (u, Q_0) in Fig. 2, $W = Q_0\, u$, or in differential term, $\mathrm{d}W = Q_0\, \mathrm{d}u$. This intuitive result follows from the definition $W = \int_0^u (\mathrm{d}W)_{|_{Q_0}}\, \mathrm{d}u = \int_0^u (Q_0\, \mathrm{d}u)_{|_{Q_0}} = Q_0 \int_0^u \mathrm{d}u = Q_0\, u$, where the subscript $_{|_{Q_0}}$ means load-controlled conditions (Q_0 fixed). The strain energy is $U = 1/2\, k\, u^2$, i.e. $1/2$ of the external work, indicated by the area of the blue triangle in Fig. 2. In differential terms, we have $\mathrm{d}U = k\, \mathrm{d}u$. Instead of calculating U from its definition, we can equivalently derive U from the knowledge of W, by using energy conservation which requires $\mathrm{d}U = \mathrm{d}W$. Thus,

$$U = \int_0^u \mathrm{d}U = \int_0^u \mathrm{d}W = \int_0^u Q_0\, \mathrm{d}u = \int_0^u k\, u\, \mathrm{d}u = \frac{1}{2}\, k\, u^2 \tag{16}$$

Critically, to obtain the correct result the integral, $\int_0^u Q_0\, \mathrm{d}u$ should not be carried out at Q_0 constant, but interpreting Q_0 as a function of u via the force–displacement relation $Q_0 = k\, u$. If the integral was calculated for Q_0 constant, we would have obtained the wrong result $U = \kappa u^2$.

In the coming section, we will apply the principle illustrated with the spring system to the calculation of the external work of follower forces. The difference is in the definition of $\mathrm{d}u$. While in the spring system, force and displacement share the same direction, in the elastica with a follower load, force and displacement are not parallel.

3.1. Shear follower force

Let us consider two infinitesimally close configurations. The infinitesimal work δW is

$$\delta W = \left(Q_0\, \hat{\mathbf{n}}_0 \cdot \mathrm{d}\mathbf{x}_0\right)_{|_{Q_0}}. \tag{17}$$

Here, $\mathrm{d}\mathbf{x}_0$ is the differential of the point of application $\mathbf{x}_0^T = \begin{bmatrix} x(S) & y(S) \end{bmatrix}_{|_{S=0}}$ of the force and $\hat{\mathbf{n}}_0^T = \begin{bmatrix} -\sin\theta_0 & \cos\theta_0 \end{bmatrix}$ is the unit vector parallel to the force. The subscript $_{|_{Q_0}}$ indicates that the magnitude of the force is kept constant, because we are considering load-controlled conditions. The load direction, however, changes during $\mathrm{d}\mathbf{x}_0$, as per definition of follower force. For this reason, δW is not an exact differential. The work done by the follower force along the trajectory γ is

$$W = \int_\gamma \left(Q_0\, \hat{\mathbf{n}}_0 \cdot \mathrm{d}\mathbf{x}_0\right)_{|_{Q_0}} = Q_0 \int_\gamma \left(\hat{\mathbf{n}}_0 \cdot \mathrm{d}\mathbf{x}_0\right) \tag{18}$$

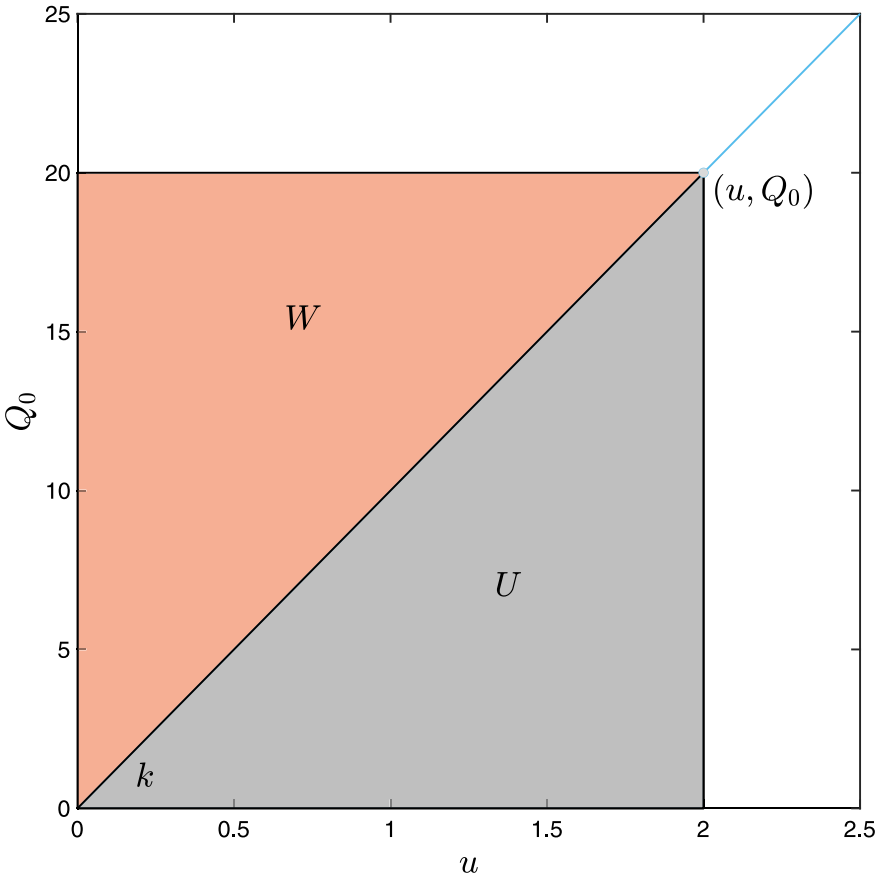

Fig. 2. External work W (rectangle) and strain energy U (blue triangle) for a spring with stiffness k displaced by u.

where γ is the trajectory of $\mathbf{x}_0$ from the undeformed configuration corresponding to $Q_0 = 0$ to the loaded configuration (Figs. 5 and 3(a) for concentrated force and Figs. 4 and 6 for distributed load). Here, as in the spring example, Q_0 is constant and therefore can be taken out of the integral. Let us parametrize the trajectory γ as $\gamma : \xi \in [0, Q_0] \rightarrow \begin{pmatrix} x_0(\xi) & y_0(\xi) \end{pmatrix}$, with $\mathrm{d}\mathbf{x}_0^T = \begin{bmatrix} \dfrac{\mathrm{d}x_0}{\mathrm{d}\xi} & \dfrac{\mathrm{d}y_0}{\mathrm{d}\xi} \end{bmatrix} \mathrm{d}\xi$.

We obtain

$$W[Q_0] = Q_0 \int_0^{Q_0} F[\xi]\, \mathrm{d}\xi \tag{19}$$

with the functional F defined as

$$F\left[Q_0\right] = -\sin\theta_0 \frac{\mathrm{d}x_0}{\mathrm{d}Q_0} + \cos\theta_0 \frac{\mathrm{d}y_0}{\mathrm{d}Q_0}. \tag{20}$$

One could solve the equilibrium Eqs. (13), obtain θ_0 and x_0 and y_0, differentiate with respect to Q_0, and perform the integration in Eq. (19) (the reader can find such solution in Appendix A). This procedure, although feasible, is terribly cumbersome. The example of the spring suggests an alternative, much simpler approach, which consists in calculating U from W.

The key is to calculate U as $U = \int_\gamma \mathrm{d}W$, and carry out the integral by interpreting Q_0 as a variable quantity. In formulas, we can simply write

$$U = \int_\gamma Q_0 \left(\hat{\mathbf{n}}_0 \cdot \mathrm{d}\mathbf{x}_0\right) = \int_0^{Q_0} \xi\, F[\xi]\, \mathrm{d}\xi. \tag{21}$$

where Q_0, unlike in Eq. (18), is kept inside the integral.

The fact that for a spring $W = 2U$, suggests that a simple relation between U and W exists also for our case of follower forces. We obtain this relation by differentiating both sides of Eq. (21) with respect to Q_0 to get $\dfrac{\mathrm{d}U}{\mathrm{d}Q_0} = \xi\, F[\xi]$. Evaluating this expression for $\xi = Q_0$ we obtain

$$F[Q_0] = \frac{1}{Q_0}\frac{\mathrm{d}U}{\mathrm{d}Q_0} \tag{22}$$

Inserting Eq. (22) into Eq. (19) and integrating by parts we finally obtain

$$\begin{aligned} W &= Q_0 \left(\int_0^{Q_0} \frac{1}{\xi}\frac{\mathrm{d}U}{\mathrm{d}\xi}\,\mathrm{d}\xi\right) = Q_0 \left(\frac{U}{Q_0} + \int_0^{Q_0} \frac{U}{\xi^2}\,\mathrm{d}\xi\right) \\ &= U + Q_0 \int_0^{Q_0} \frac{U}{\xi^2}\,\mathrm{d}\xi. \end{aligned} \tag{23}$$

For a spring and in general for small deflections the last integral reduces to U, as it will be demonstrated shortly.

Eq. (23) provides a practical formula for computing the external work. The strain energy has an explicit expression, as shown in Appendix A, and we shall assume it a known quantity. The external work is then the sum of the strain energy and an integral over the strain energy. The integral in Eq. (23) does not seem to have a closed-form solution in its general form; hence, we computed it numerically with an adaptive scheme (Shampine, 2008).

At first glance, it might appear that the integral in Eq. (23) is singular for $Q_0 = 0$. However, for small Q_0 and from Eq. (A.20), $U\left[Q_0\right] = \sqrt{2\,Q_0}\, I_2\left(\bar{\mu}_1\right)$, with $\bar{\mu}_1$ being the curvature at the root ($S = 1$). Also, for small Q_0, $I_2\left(\bar{\mu}_1\right) \approx \frac{1}{3}\,\bar{\mu}_1^3$, hence $U[Q_0] \approx 1/6\, {Q_0}^2$. Substituting into Eq. (23), we get

$$W = U + Q_0 \int_0^{Q_0} \frac{U}{\xi^2}\,\mathrm{d}\xi = U + Q_0 \int_0^{Q_0} \frac{1}{6}\,\mathrm{d}\xi = U + \frac{1}{6}\,{Q_0}^2 = 2\,U\,, \tag{24}$$

which is Clapeyron's theorem.

If the load has a fixed direction (Fig. 3(b)), then $\hat{\mathbf{n}}_0^T = \begin{bmatrix} 0 & 1 \end{bmatrix}$, therefore

$$W = Q_0 \int_0^{Q_0} \frac{\mathrm{d}y_0}{\mathrm{d}\xi}\,\mathrm{d}\xi = Q_0 \int_0^{y_0} \mathrm{d}y_0 = Q_0\, y_0\,, \tag{25}$$

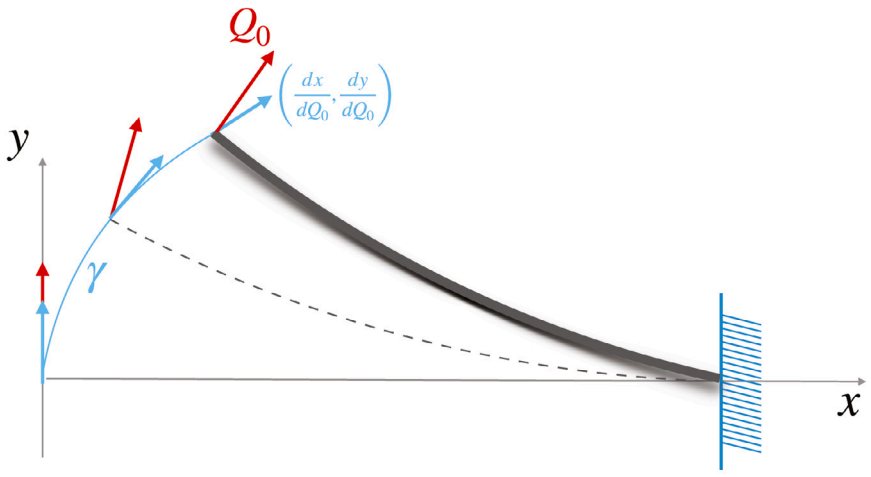

(a) Follower Force

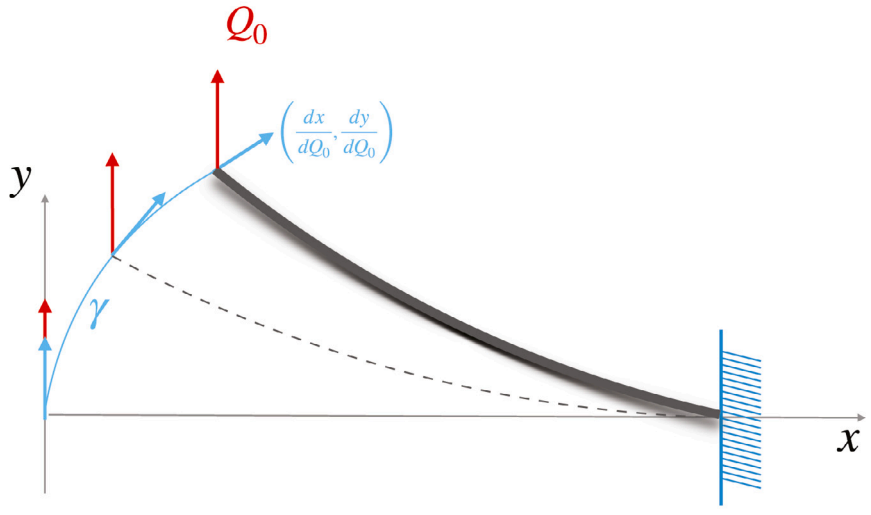

(b) Fixed Force

Fig. 3. External work by a follower (a) and fixed (b) load. The thick black line is the deformed rod at load Q_0. The thin blue line is the trajectory γ of the point of application of the shear force, from zero load to an arbitrary value Q_0. The red arrow is the follower force, whose magnitude is kept constant. The blue arrow is the tangent vector to the trajectory.

which is the familiar expression "force times displacement in the direction of the force".

3.2. Uniform follower pressure

The infinitesimal work δW for a distributed load can be formulated similarly to Eq. (17):

$$\delta W = \left(q \int_0^1 \hat{\mathbf{n}}(S) \cdot \mathrm{d}\mathbf{x}\, \mathrm{d}S \right)_{|_q} = q\, F[q]\, \mathrm{d}q\,, \tag{26}$$

where

$$F[q] = \int_0^1 -\sin\theta \frac{\mathrm{d}x}{\mathrm{d}q} + \cos\theta \frac{\mathrm{d}y}{\mathrm{d}q}\, \mathrm{d}S\,. \tag{27}$$

In load-controlled conditions, where the subscript $_{|_q}$, means fixed q between two infinitesimally close deformations, the total work is

$$W = \int_0^q (\delta W)_{|_q} = q \int_0^q F[\xi]\, \mathrm{d}\xi\,. \tag{28}$$

Because of conservation of energy, the following equality (*without* keeping the load q fixed) holds

$$U = \int_0^q \delta W = \int_0^q \xi\, F[\xi]\, \mathrm{d}\xi\,. \tag{29}$$

Substituting

$$F[q] = \frac{1}{q} \frac{\mathrm{d}U}{\mathrm{d}q}\,. \tag{30}$$

into Eq. (28), and integrating by parts, we get

$$W = q \left(\frac{U}{q} + \int_0^q \frac{U}{\xi^2}\, \mathrm{d}\xi \right) = U + q \int_0^q \frac{U}{\xi^2}\, \mathrm{d}\xi\,. \tag{31}$$

We notice that Eqs. (23) and (31) are identical, with the only difference being the functional expression of U.

Eq. (31) reduces to the Clapeyron theorem for $q \ll 1$. To show this, we start from the equation defining implicitly the solution in the re-scaled variable $\bar{\mu}$ (see Appendix B for the full expression)

$$2\sqrt{\bar{\mu}_1}\, {}_2F_1\left(\frac{1}{6}, \frac{1}{2}; \frac{7}{6}; \bar{\mu}_1^3\right) - q^{1/3} = 0\,. \tag{32}$$

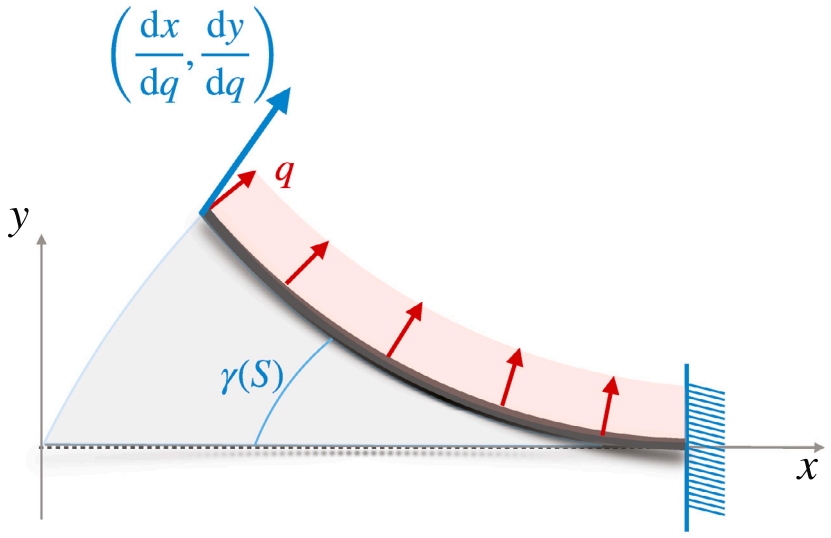

Fig. 4. External work by a follower distributed uniform load. The thick black line is the deformed rod at load q. The thin blue line is the trajectory $\gamma(S)$ of the point S of the rod. They gray area is the (continuum) union of all the trajectories $\gamma(S)$. The red arrow is the follower force, whose magnitude is kept constant. The blue arrow is the tangent vector to the trajectory.

For small q also $\bar{\mu}_1$ is small. We can therefore expand the first term of Eq. (32) in Puiseux series

$$2\sqrt{\bar{\mu}_1}\,{}_2F_1\left(\frac{1}{6},\frac{1}{2};\frac{7}{6};\,\bar{\mu}_1^3\right) = 2\sqrt{\bar{\mu}_1} + O(\bar{\mu}_1^{7/2}). \tag{33}$$

Similarly, we can expand the strain energy (Eq. (B.13)) in Puiseux series and using the approximation $2\,\bar{\mu}_1^{1/2} \approx q^{1/3}$

$$U \approx \frac{4}{5}\,\frac{1}{2^5}\,q^{1/3}\,q^{5/3} = \frac{1}{40}\,q^2\,, \tag{34}$$

This result can also be obtained by assuming a linear theory for a beam under an uniform load.

Substituting Eq. (34) into Eq. (31) recovers the Clapeyron theorem:

$$W = U + q\int_0^q \frac{U}{\xi^2}\,\mathrm{d}\xi = U + q\int_0^q \frac{1}{40}\,\mathrm{d}\xi = U + \frac{1}{40}\,q^2 = 2\,U\,. \tag{35}$$

In the case of distributed load acting on a fixed direction, the work (31) becomes

$$W = q\int_0^q \mathrm{d}\xi\int_0^1 \frac{\mathrm{d}y}{\mathrm{d}\xi}\mathrm{d}S = q\int_0^1 \mathrm{d}S\int_0^q \frac{\mathrm{d}y}{\mathrm{d}\xi}\mathrm{d}\xi = q\,y_P(q)\,, \tag{36}$$

where $y_P(q)$ is the y-coordinate of the *center of pressure*

$$y_P(q) = \int_0^1 y(S,q)\,\mathrm{d}S\,. \tag{37}$$

That is, the work is the constant load multiplied by the y-coordinate of the center of pressure.

3.3. Tangential follower force

We finally consider the case of Kendall peeling (Kendall, 1971, 1975), where the angle θ_0 is fixed (Fig. 7).

$$W\left[N_0\right] = N_0\int_0^{N_0} F\left[\xi\right]\,\mathrm{d}\xi \tag{38}$$

with the functional F defined as

$$F\left[N_0\right] = \cos\theta_0\,\frac{\mathrm{d}X_0}{\mathrm{d}N_0} + \sin\theta_0\,\frac{\mathrm{d}Y_0}{\mathrm{d}N_0} \tag{39}$$

where subscript $_0$ refers to the tip of the elastica, and X and Y are the Cartesian coordinates shown in Fig. 7. Since θ_0 is fixed, the integral in the right hand side of Eq. (38) is readily computed as

$$W\left[N_0\right] = N_0\left(\cos\theta_0\,(X_0-1) + \sin\theta_0\,Y_0\right) \tag{40}$$

In the limit of $N_0 \to \infty$, $X_0 = \cos\theta_0$ and $Y_0 = \sin\theta_0$, and Eq. (40) returns Rivlin's formula $W\left[N_0\right] = N_0\left(1-\cos\theta_0\right)$ (Rivlin, 1944; Kendall, 1971).

The strain energy is given by Eq. (C.9). The full solution is reported in Appendix C.

3.4. Remark

We conclude this section by noting that, in all the cases examined here, the external work is given by the same formula, either equation (23) or (31). Using the same arguments, one could easily show that Eqs. (23) and (31) hold also for the cases with fixed loads. However, in such cases, the work is more readily computed through Eqs. (25), (36) and (40). It is interesting to notice, however, that a general formula of the type of (23) seems to include all the cases, both for follower and fixed loads.

4. Strain energy release rate

We now utilize the results in Sections 3.1 and 3.2 to obtain general expressions for the strain energy release rate G.

The dimensionless potential energy and dimensionless strain energy release rate satisfy Π^* is $\Pi^* = \frac{\Pi\,L}{E\,I}$ and $G = \frac{E\,I}{b}\,\frac{1}{L^2}\,G^*$. Using Eq. (2), we obtain

$$G = \frac{E\,I}{b\,L^2}\left(-(-\Pi^*) + L\,\frac{\partial(-\Pi^*)}{\partial L}\right) \tag{41}$$

Using the fact that Π^* depends on ${M_0}^*, {Q_0}^*, {N_0}^*, q^*$ (given by Eq. (8)) and applying the chain rule. we get:

$$G^* = \frac{\partial(-\Pi^*)}{\partial {M_0}^*}\,{M_0}^* + 2\frac{\partial(-\Pi^*)}{\partial {Q_0}^*}\,{Q_0}^* + 2\frac{\partial(-\Pi^*)}{\partial {N_0}^*}\,{N_0}^* + 3\frac{\partial(-\Pi^*)}{\partial q^*}\,q^* - (-\Pi^*)\,. \tag{42}$$

This expression shows that we do not need to solve the full elastic problem to calculate G, but only know how Π depends on ${M_0}^*, {Q_0}^*, {N_0}^*, q^*$. Using the results of the previous sections, we now consider the specific cases of follower shear force, follower uniform pressure and follower tangential force. For the case of shear follower force, we have

$$-\Pi = Q_0\int_0^{Q_0} \frac{U}{\xi^2}\,\mathrm{d}\xi \tag{43}$$

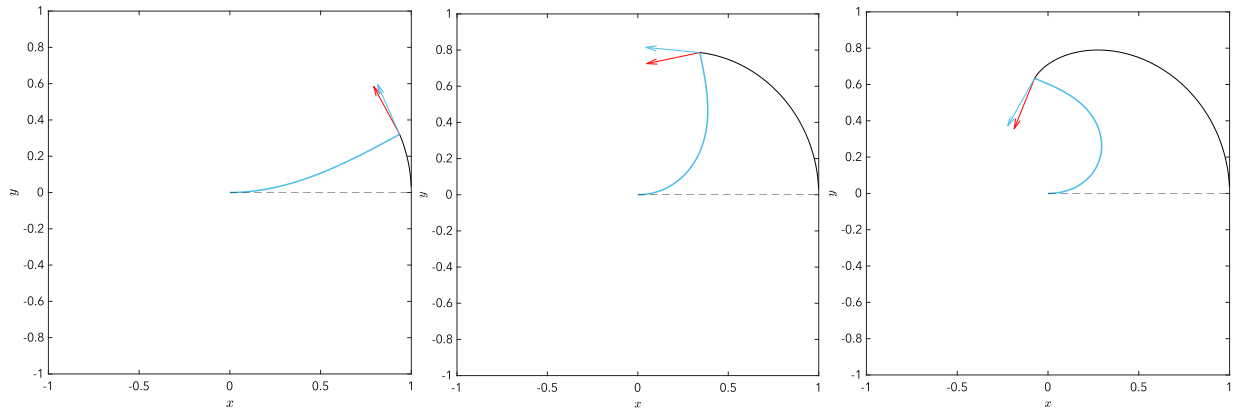

(a) $Q_0 = 0.1$ (b) $Q_0 = 4$ (c) $Q_0 = 8$

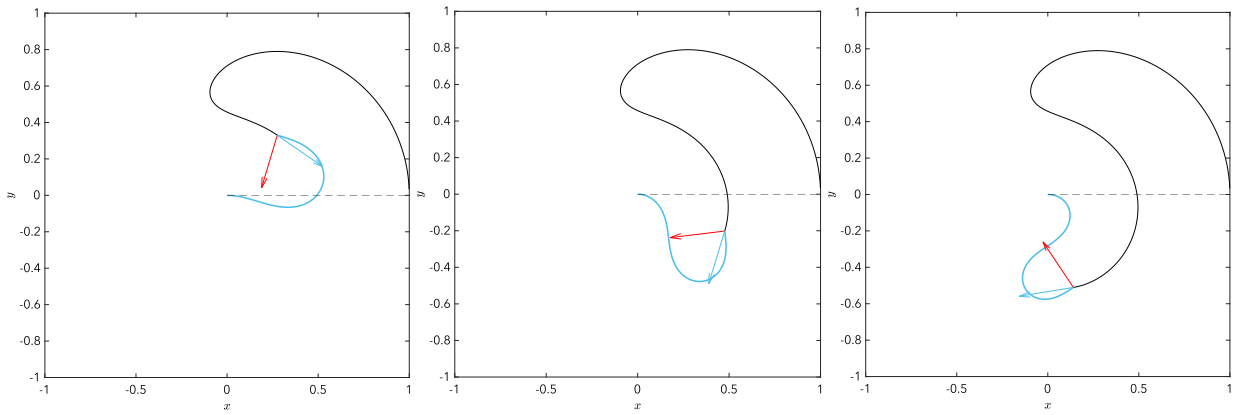

(d) $Q_0 = 20$ (e) $Q_0 = 30$ (f) $Q_0 = 40$

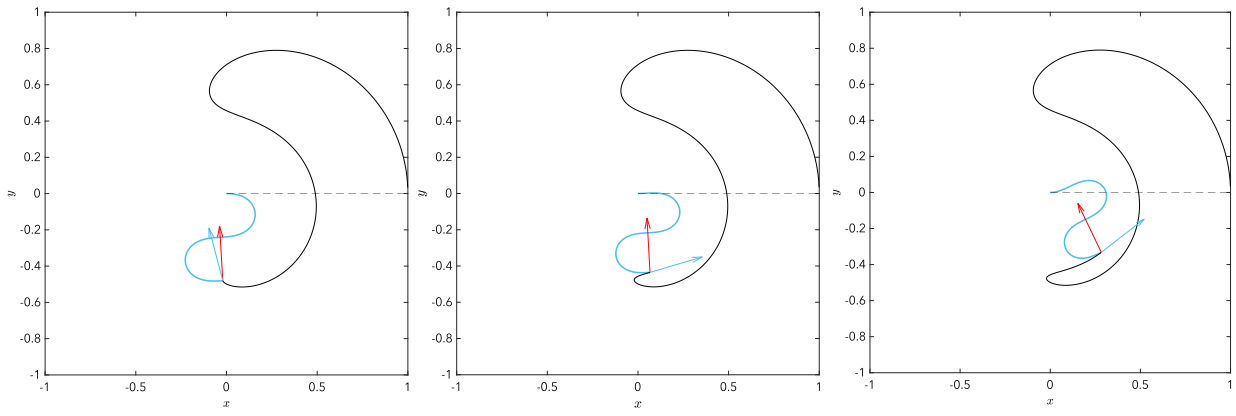

(g) $Q_0 = 50$ (h) $Q_0 = 60$ (i) $Q_0 = 70$

Fig. 5. Deformation (blue line) of the elastica under a shear follower force (red arrow). The black line is the trajectory γ of the free end; the blue arrow is the tangent to γ.

and

$$Q_0 \frac{\partial(-\Pi)}{\partial Q_0} = U + Q_0 \int_0^{Q_0} \frac{U}{\xi^2}\,\mathrm{d}\xi = W \tag{44}$$

hence

$$G = 2\,Q_0 \frac{\partial(-\Pi)}{\partial Q_0} - (-\Pi) = 2\,W - (W - U) = W + U \tag{45}$$

Where we have omitted the superscript * to ease the notation. For the case of the uniform follower load:

$$-\Pi = q \int_0^q \frac{U}{q^2}\,\mathrm{d}\xi \tag{46}$$

and

$$q \frac{\partial(-\Pi)}{\partial q} = U + q \int_0^q \frac{U}{\xi^2}\,\mathrm{d}\xi = W \tag{47}$$

Hence:

$$G = 3\,q \frac{\partial(-\Pi)}{\partial q} - (-\Pi) = 3\,W - (W - U) = 2\,W + U \tag{48}$$

For a fixed shear force, $W = Q_0\,y_0$, (Eq. (25)). To get the strain energy, one could, in principle, solve the elastica for a terminal shear fixed force, and integrate the square of the curvatures; such solution is

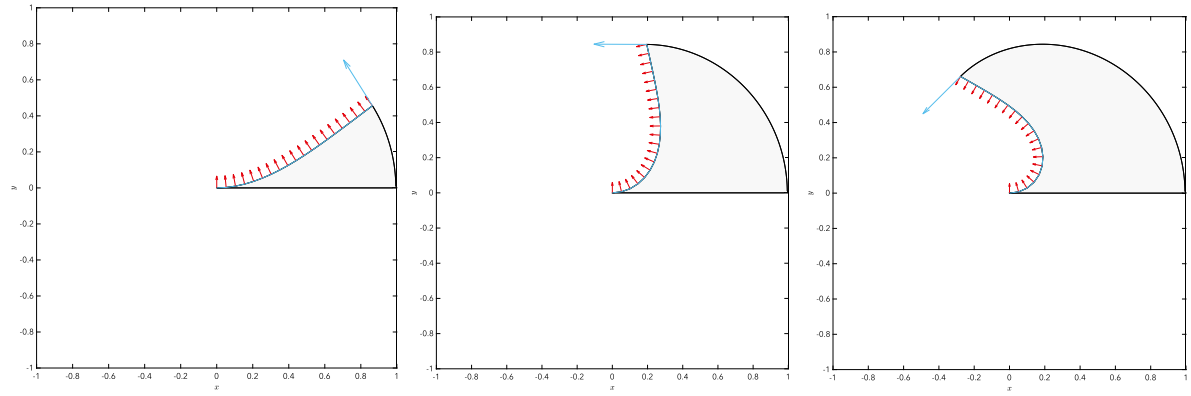

(a) $q = 4$ (b) $q = 12$ (c) $q = 20$

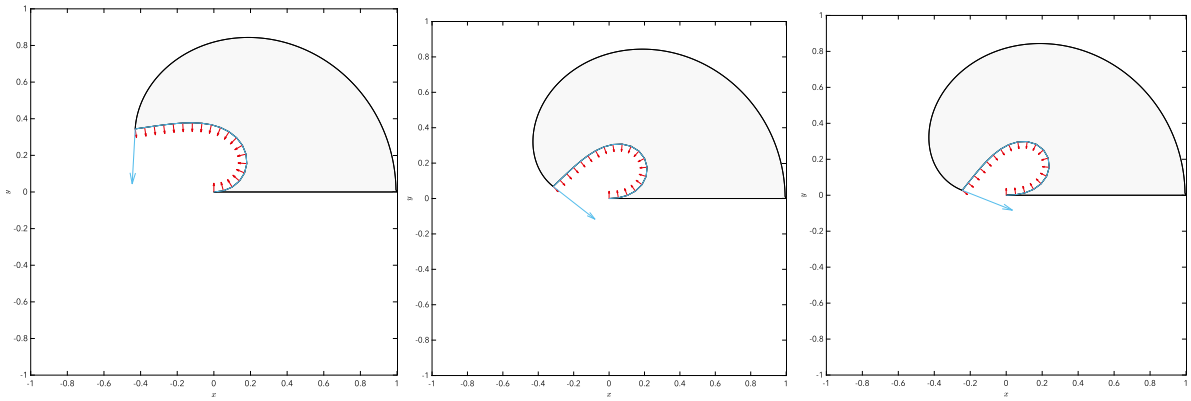

(d) $q = 30$ (e) $q = 50$ (f) $q = 60$

Fig. 6. Deformation (blue line) of the elastica under a distributed uniform follower load (red arrow). The gray area is the union of all the trajectories of the points of the rod; the blue arrow is the tangent to the trajectory for $S = 0$.

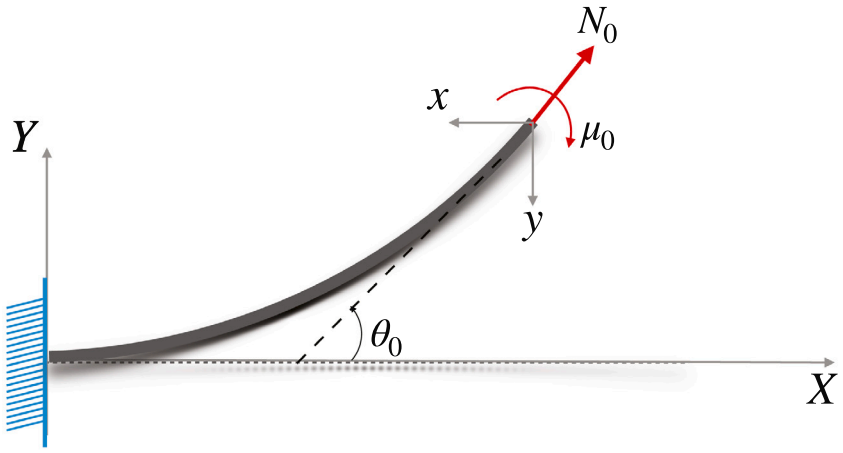

Fig. 7. Peeling due to a terminal tangential follower force N_0 with a tip angle θ_0. The tip curvature μ_0 depends on N_0 and θ_0 through Eq. (C.6).

expressed through Jacobi elliptic functions (Frisch-Fay, 1962; Bigoni, 2012). We follow here a different approach.

Using the non-dissipative nature of non-conservative forces we have

$$U = \int_0^{Q_0} Q_0 \, \frac{\mathrm{d}y_0}{\mathrm{d}Q_0} \, \mathrm{d}Q_0 \tag{49}$$

The derivative of the potential energy with respect to Q_0 is

$$\frac{\partial(-\Pi)}{\partial Q_0} = y_0 + Q_0 \, \frac{\mathrm{d}y_0}{\mathrm{d}Q_0} - Q_0 \, \frac{\mathrm{d}y_0}{\mathrm{d}Q_0} = y_0 \tag{50}$$

Hence, the strain energy release rate is

$$G = 2\,Q_0 \, \frac{\partial(-\Pi)}{\partial Q_0} - (-\Pi) = 2\,Q_0\,y_0 - Q_0\,y_0 + \int_0^{Q_0} Q_0 \, \frac{\mathrm{d}y_0}{\mathrm{d}Q_0} \, \mathrm{d}Q_0 = W + U \tag{51}$$

For a fixed uniform pressure, the work done by the external forces is given by Eq. (36), i.e. $W = q\,y_P(q)$ with $y_P(q)$ being the center of pressure (37).

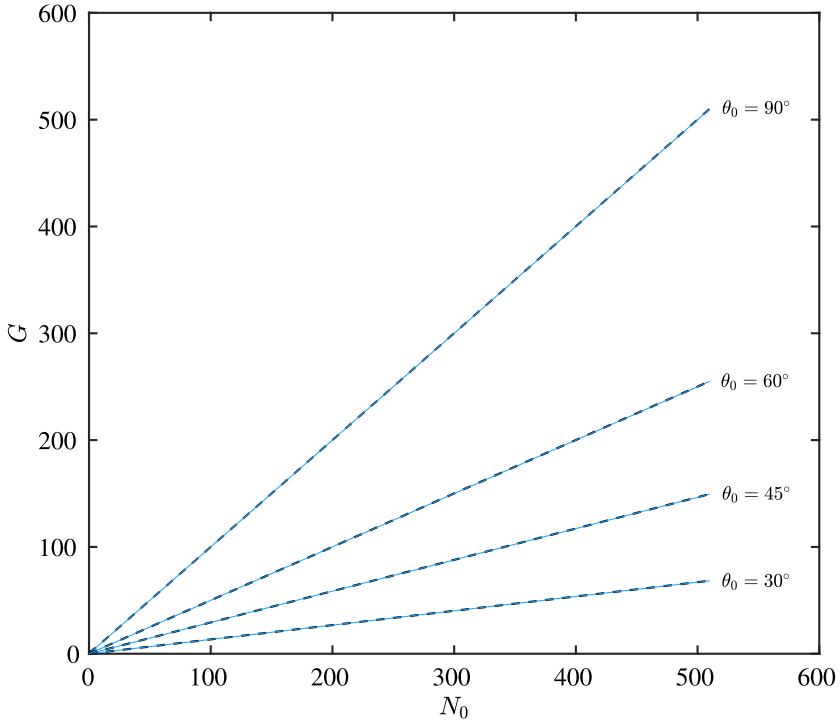

Fig. 8. Strain Energy Release Rate for the Kendall peeling: comparison between Eq. (57) (continuous line) and Rivlin's formula $G = (1 - \cos\theta_0)\, N_0$ (dashed line).

The strain energy is

$$U = \int_0^1 \mathrm{d}S \int_0^q \xi \frac{\mathrm{d}y}{\mathrm{d}\xi}\,\mathrm{d}\xi \tag{52}$$

and the derivative of the potential energy with respect to q is

$$\begin{aligned}\frac{\partial(-\Pi)}{\partial q} &= y_P(q) + q\frac{\mathrm{d}y_P}{\mathrm{d}q} - \int_0^1 q\frac{\mathrm{d}y}{\mathrm{d}q}\mathrm{d}S \\ &= y_P(q) + \int_0^1 q\frac{\mathrm{d}y}{\mathrm{d}q}\,\mathrm{d}S - \int_0^1 q\frac{\mathrm{d}y}{\mathrm{d}q}\mathrm{d}S = y_P(q)\end{aligned} \tag{53}$$

Therefore, the strain energy release rate is

$$G = 3\,q\frac{\partial(-\Pi)}{\partial q} - (-\Pi) = 3\,q\,y_P(q) - W + U = 3W - W + U = 2\,W + U \tag{54}$$

Finally, for the case of a tangential follower force (Kendall peeling), we have that

$$U = \int_0^{N_0} N_0 \left(\cos\theta_0 \frac{\partial X_0}{\partial N_0} + \sin\theta_0 \frac{\partial Y_0}{\partial N_0}\right) \mathrm{d}N_0 \tag{55}$$

where θ_0 is fixed. The derivative of the potential energy with respect to N_0 is

$$\begin{aligned}\frac{\partial(-\Pi)}{\partial N_0} &= \cos\theta_0\,\left(X_0 - 1\right) + \sin\theta_0\, Y_0 + N_0\left(\cos\theta_0\frac{\partial X_0}{\partial N_0} + \sin\theta_0\frac{\partial Y_0}{\partial N_0}\right) \\ &\quad - N_0\left(\cos\theta_0\frac{\partial X_0}{\partial N_0} + \sin\theta_0\frac{\partial Y_0}{\partial N_0}\right) = \\ &= \cos\theta_0\,\left(X_0 - 1\right) + \sin\theta_0\, Y_0\end{aligned} \tag{56}$$

Therefore

$$\begin{aligned}G &= 2\,N_0\frac{\partial(-\Pi)}{\partial N_0} - (-\Pi) = 2\,N_0\,\left(\cos\theta_0\,\left(X_0 - 1\right) + \sin\theta_0\, Y_0\right) - W + U \\ &= 2\,W - W + U = W + U\end{aligned} \tag{57}$$

In Eq. (57) we have neglected the term $\frac{\partial(-\Pi)}{\partial M_0} M_0$ since $M_0 \to 0$ for large loads. Fig. 8 shows an excellent match between the strain energy release computed through Eqs. (38), (57) and (C.9) for different θ_0 angles.

We also notice that the expressions for loads of fixed directions are found to be identical to the ones for follower loads.

4.1. Geometrical and physical interpretation of the external work

We now look at the formulas derived in Sections 3.1–3.3 in the context of the spring system example at the beginning of Section 3. Let us focus for simplicity on the follower concentrated force. We can define the *effective displacement* u as

$$u = \int_0^{Q_0} F[\xi]\,\mathrm{d}\xi \tag{58}$$

Therefore, according to the definition (19), the external work can be expressed simply as

$$W = Q_0\, u \tag{59}$$

Graphically, W is the area of the rectangle in Fig. 9 in the plane $u - Q_0$. The area under the curve $Q_0 = Q_0(u)$ is the strain energy: indeed, from Eq. (58)

$$\mathrm{d}u = F[Q_0]\,\mathrm{d}Q_0 \tag{60}$$

$$\int_0^u Q_0(u)\,\mathrm{d}u = \int_0^{Q_0} \xi\, F[\xi]\,\mathrm{d}\xi = U \tag{61}$$

where we used Eq. (21). Therefore, the red area in Fig. 9 is $-\Pi$. The dashed curve in Fig. 9 is the small displacements approximation

$$Q_0 = 3\,u \tag{62}$$

5. Comparison between critical follower and fixed loads

We computed the strain energy release rate for the peeling with follower shear force and follower uniform pressure to calculate the critical load for peeling. In the literature, the following results exist for large deformation peeling: Rivlin first and Kendall independently (Rivlin, 1944; Kendall, 1971, 1975) used an *inextensible fabric* approximation and found that the critical load F necessary to peel off an adhesive strip with *no bending rigidity* perpendicularly from a substrate is $F = \Gamma\, b$. For a strip with no bending rigidity and finite membrane rigidity, Kendall showed $F\,(1 + \epsilon/2) = \Gamma\, b$, where the axial strain is $\epsilon = F/(E\,t\,b)$, with

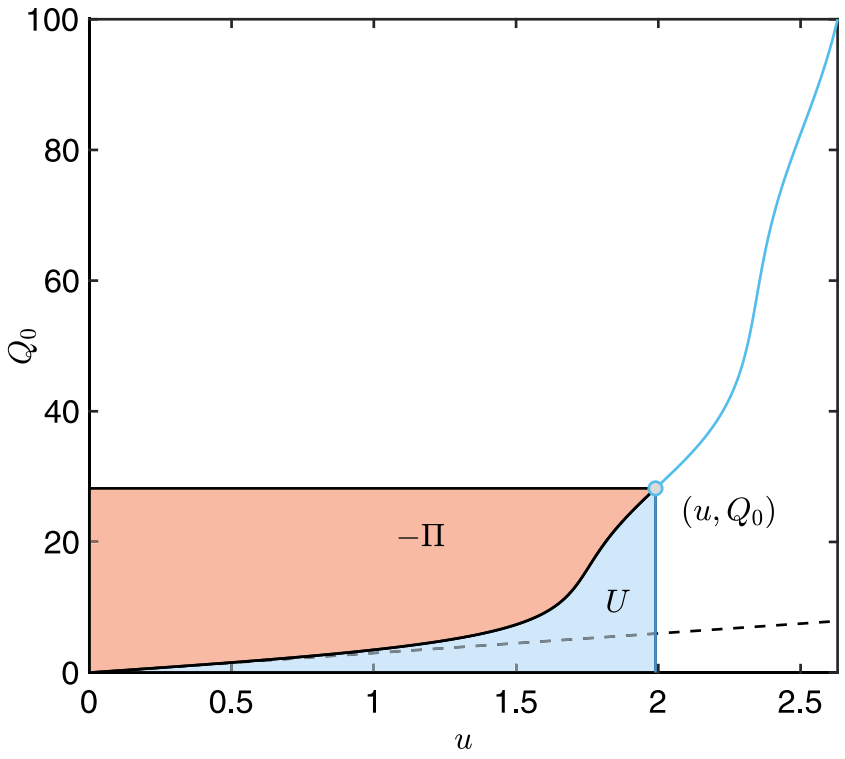

Fig. 9. Geometrical and physical interpretation of the strain energy U, potential energy Π and external work W. The axis u is the effective displacement. The blue area under the curve $Q_0 = Q_0(u)$ is the strain energy. The red area is $-\Pi$. The sum of the two areas is the area of the rectangle having (u, Q_0) as a vertex and is the external work. The dashed line is the small displacements limit $Q_0 = 3\,u$.

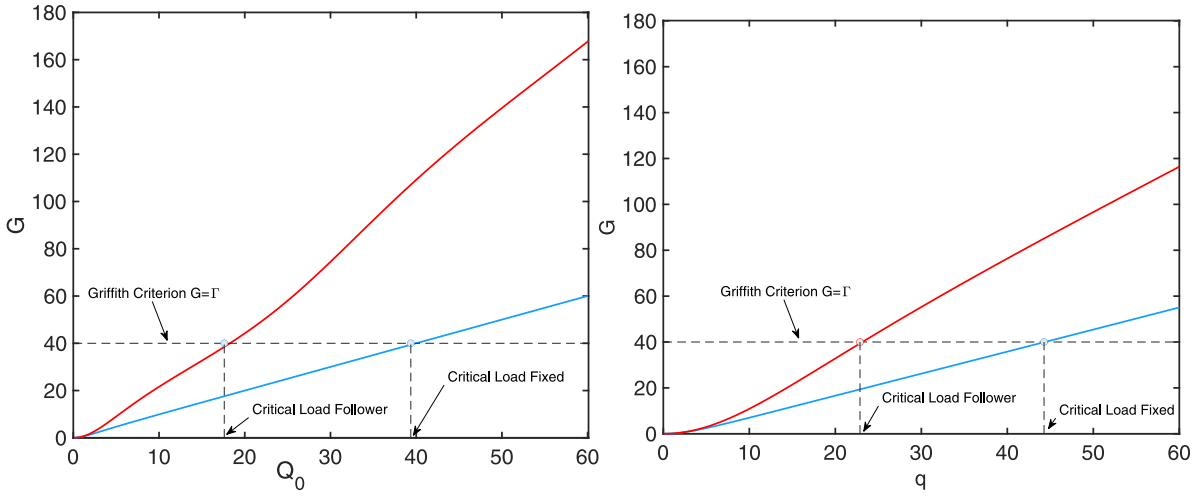

(a) Shear Force $G = W + U$ (b) Uniform Pressure $G = 2\,W + U$

Fig. 10. Strain Energy Release Rate for peeling with follower forces (red curves) and fixed forces (blue curves).

t being the thickness of the strip. For inextensible strips with finite bending rigidity at large deformations, the same result applies. For large Γ, using the Euler's inextensible elastica, Roman (2013) showed that $F = \Gamma\, b$ for an elastica loaded by a terminal axial load parallel to the deformation of the strip. Such a case can be considered as a follower *tangential* load. We proved that the approach proposed in this paper matches Rivlin's formula for peeling at different angles perfectly. For the case of follower *perpendicular* loads we find for large Γ a similar result to (Rivlin, 1944; Kendall, 1971, 1975) for $\theta_0 = \pi/2$.

We start by finding that for the shear force, $G = W + U$, and for the pressure, $G = 2\,W + U$. Appendices A and B contain the expressions for the strain energy U, while Sections 3.1 and 3.2 described the procedure to obtain W. These formulas for the external work are one of the main achievements of this paper.

We also compared each case with the strain energy release rates of peeling with fixed loads. Even though the expressions for G are the same as the follower case, the computation of the external work is much simpler conceptually, as it is "force times displacement". The strain energy U for the case of the shear force is obtainable analytically thanks to well-known solutions of the elastica. For the distributed case, a solution through a power series expansion exists (Rohde, 1953).

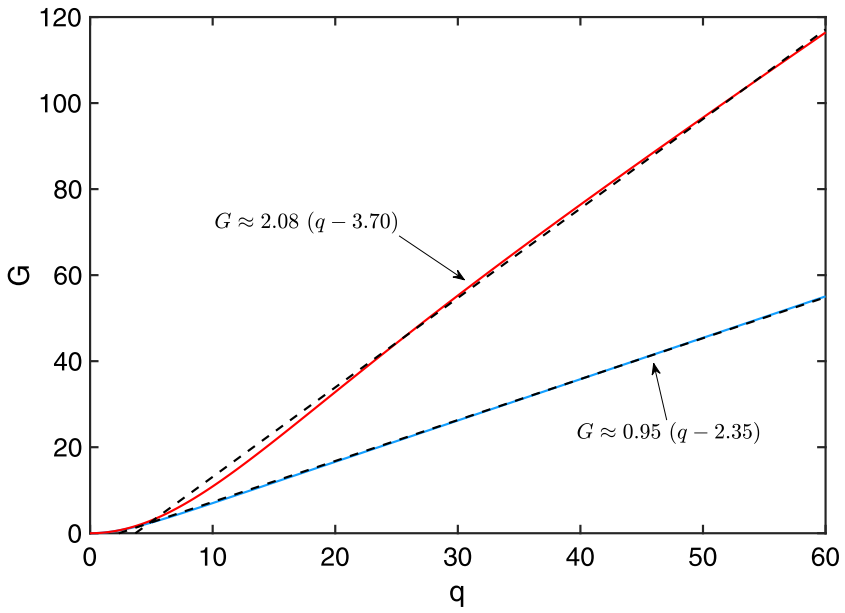

Fig. 11. Strain Energy Release Rate for peeling with uniform pressure: $G \approx C\,(q - q_{SD})$ for $q > q_{SD}$. In dimensional form, this implies that the critical load $q_c \sim \Gamma\, L^{-1}$. Red curve is G for follower loads, blue curve is G for fixed loads. Dashed lines are the linear fits.

Figs. 10 compare these four curves for varying loads. For the Griffith energy balance

$$G = \Gamma \tag{63}$$

where Γ is the solid–solid interface energy and G is the *strain energy release rate* (Eq. (2)). The Griffith criterion is a horizontal curve on these graphs, intercepting the G-curves at the critical loads. We can see that the critical follower loads are lower than the critical fixed loads. Critical loads depend on critical shear rates, which in turn rely on the power necessary to generate shear flows (Salussolia et al., 2020; Botto, 2019).

To quantify how lower critical follower loads are than the fixed ones, let us focus on the peeling with uniform pressure. For large q, G approximately follows a law $G \approx C\,(q - q_{SD})$, with q_{SD} interpreted as the limit of validity for the small displacements assumption. Indeed, for follower pressure, $q_{SD} = 3.70$, at which value the load and the tangent of the trajectory are still parallel (Fig. 6(a)). From this linear fit, using the Griffith criterion, we can derive that the critical load q_c for peeling initiation is

$$\begin{aligned} q_c &= 0.48\,\Gamma\, L^{-1} \quad \text{follower,} \\ q_c &= 1.05\,\Gamma\, L^{-1} \quad \text{fixed,} \end{aligned} \tag{64}$$

where we have used the dimensional form (see Fig. 11).

Also, the ratio between the two critical loads is $\frac{q_c^{\text{follower}}}{q_c^{\text{fixed}}} = 0.45$

Similarly, for the case with shear forces

$$\begin{aligned} Q_{0_c} &= 0.32\,\Gamma \quad \text{follower,} \\ Q_{0_c} &= \Gamma \quad \text{fixed,} \end{aligned} \tag{65}$$

where Q_{0_c} is the applied force per unit width. The ratio between the critical loads is $\frac{Q_{0_c}^{\text{follower}}}{Q_{0_c}^{\text{fixed}}} = 0.32$ For completeness, the critical loads for fixed direction and small displacements are (in dimensional form)

$$\begin{aligned} q_c &= \frac{1}{L^2}\sqrt{\frac{E\,I}{b}}\sqrt{8}\sqrt{\Gamma} \quad \text{pressure} \\ Q_{0_c} &= \frac{1}{L}\sqrt{\frac{E\,I}{b}}\sqrt{2}\sqrt{\Gamma} \quad \text{shear} \end{aligned} \tag{66}$$

6. Application to hydrodynamic peeling in graphene production

As an illustrative application, we consider a simple hydrodynamic peeling model for the estimation of critical shear rates in liquid exfoliation processes for the production of graphene from graphite (Paton et al., 2014). In this widely applied liquid-based process, coarse graphite particles are dispersed in a suitable liquid solvent and subject to energetic mechanical mixing for several hours. The processing flow is typically turbulent. Suppose the liquid solvent can intercalate between the graphite particle's graphene layers. In that case, the pressure forces produced by the fluid can lift layers of graphite, gradually eroding the mother graphite particle by what was referred to, in a previous publication, as a mechanism of "hydrodynamic peeling" (Salussolia et al., 2020). For small peeling velocities, the hydrodynamic peeling process is quasi-static and the fluid pressure p, acting normally to the instantaneous lifted layer surface, can be considered uniform and follower with good approximation . We can use our theory and write $q_c = p \simeq \mu\dot{\gamma}$, where μ is the dynamic viscosity of the fluid and $\dot{\gamma}$ is the instantaneous, ambient shear rate "seen" by the mother graphite particle along its Lagrangian trajectory. This expression is valid for particles smaller than the smallest scales of the turbulence (the Kolmogorov scale in liquid-phase exfoliation is $\sim 10 - 100\,\mu$m, depending on the liquid volume and applied mixing power). Using expression (64) developed for follower loads, we get the following critical shear rate:

$$\dot{\gamma} \simeq 0.48\frac{\Gamma}{\mu L} \tag{67}$$

Although accurate experimental data on critical shear rates in liquid-phase exfoliation are scarce, the scaling suggested by Eq. (67) is compatible with experimental measurements of the average exfoliated particle size L vs mixer rotor speed in a well-controlled liquid-exfoliation experiment (Paton et al., 2014). Note that because of the extremely low bending stiffness of graphene ($\sim 7eV$ or $\sim 10^{-18}$ N m) (Lindahl et al., 2012), comparable to that of tenuous biological membranes), the use of a large displacements expression is almost mandatory to explain peeling thresholds when the flap has a curvature comparable to the inverse of the crack length. The use of a small-displacement theory would give a completely different scaling for L (compare (66) with (64)). Follower and non-follower large-displacements expressions give the same scaling with respect to L, but using the non-follower expression, we get a critical shear rate more than two times larger than that predicted by Eq. (67). In terms of mixing power, this corresponds to a difference by a factor of 4. In a practical application, using the more accurate follower-load prediction would enable choosing a mixer with the right power, significantly reducing the energy requirements. Furthermore, using a mixing power that does not exceed that required for exfoliation would reduce the number of defects in the produced graphene material.

7. Conclusions

We proposed a general theoretical approach for calculating the external work for peeling off a thin layer subjected to large deformations when the load follows the structure. We considered strips subject to a terminal shear force, terminal tangential force and uniform pressure. The sheet is assumed to be inextensible and unshearable but has finite bending rigidity.

By using the theory of the elastica, we were able to obtain explicit expressions for the strain energy U. Combining this result with the external work W computation, we arrived at simple expressions for the strain energy release rate G. Specifically, in dimensionless form, we found that for the case with shear forces, $G = U + W$ and for the uniform pressure $G = U + 2W$. This result can be derived easily for small deformations, which means a regime with low interface energy. However, this paper proves the remarkable fact that the same formula holds for both fixed and follower loads causing large deformations. The key step in achieving this result is in calculating W, which we obtain in this article.

From the strain energy, we calculate the critical loads q_c (for terminal shear) and Q_{0c} (for pressure) for initiation of the fracture using Griffith's theory. For tough interfaces ($\Gamma\, b\, L^2/E\, I \gg 1$, with Γ being the solid–solid interface energy), we recover the *inextensible fabric zero-bending stiffness approximation* of Kendall and finite bending stiffness result (Roman, 2013) for axial loads: for the critical load depending linearly on Γ. However, the major result here stands also for non-axial loads, namely shear force and uniform pressure and in the different pre-factor between fixed and follower loads. Indeed, we found that the critical follower shear force is about $1/3$ of the fixed one, and that the critical follower pressure is about half than the fixed one. In liquid-exfoliation for the production of graphene from graphite, the force that determines the microscopic peeling is essentially the pressure of the fluid in the gap between an exfoliated layer and the mother particle, and the problem is typically to calculate the critical shear rate (proportional to the pressure via the viscosity) to obtain exfoliation. In this problem, assuming a fixed-direction load would lead to a gross over-prediction (up to a factor of 2) of the applied shear rate. Although specific, this example illustrates how important it is to consider the follower nature of the load.

The analysis we have carried out is for follower loads that are constant in magnitude. The general framework we have developed could be extended to include more general loads, such as the case of a load that follows a polynomial function of the distance along the strip.

Declaration of competing interest

The authors declare that they have no known competing financial interests or personal relationships that could have appeared to influence the work reported in this paper.

Acknowledgments

LB has received funding from the European Research Council (ERC) under the European Union's Horizon 2020 research and innovation program (Grant agreement No. 715475, project FLEXNANOFLOW).

Appendix A. *Elastica* loaded by a follower shear force: analytical solution

For this case, we use the approach derived in Misseroni et al. (2021).

$$\mu_0' = Q_0\,, \qquad N_0 = 0\,, \qquad \mu_0 = M_0 = 0\,, \qquad q = 0. \tag{A.1}$$

The Eq. (11) becomes

$$\mu'^2 + \frac{\mu^4}{4} - {Q_0}^2 = 0. \tag{A.2}$$

We then consider a cantilever rod, with the origin of the Cartesian system at the free end:

$$\theta(1) = 0\,, \qquad x(1) = 1\,, \qquad y(1) = 0. \tag{A.3}$$

The solution of Eq. (A.2) is a periodic solution with quarter-period $S_{\max}$ that oscillates between $-\mu_{\max}$ and $\mu_{\max}$

$$\mu_{\max} = \sqrt{2\,Q_0}\,, \qquad S_{\max} = \frac{2\,K(-1)}{\mu_{\max}} = \sqrt{\frac{2}{Q_0}}\,K(-1), \tag{A.4}$$

with $K(-1)$ being the *complete elliptical integral of the first kind* of argument -1. Let us then normalize the curvature and the curvilinear abscissa

$$\bar{S} = \frac{S}{S_{\max}}\,, \qquad \bar{\mu} = \frac{\mu}{\mu_{\max}}. \tag{A.5}$$

The solution is then

$$\bar{\mu}(\bar{S}) = \mathrm{sn}\left(K(-1)\,\bar{S}|-1\right)\,, \tag{A.6}$$

$$\bar{\mu}'(\bar{S}) = K(-1)\,\mathrm{cn}\left(K(-1)\,\bar{S}|-1\right)\,\mathrm{dn}\left(K(-1)\,\bar{S}|-1\right)\,, \tag{A.7}$$

with sn, cn and dn being respectively *Jacobi sn, cn and dn elliptic functions*.

The rotation is

$$\theta(S) = \beta_1 - \beta(S)\,, \qquad \beta_1 = \beta(1) = \theta_0\,, \tag{A.8}$$

with

$$\beta(\bar{S}) = \arcsin\left(\bar{\mu}^2\right)\,\mathrm{sign}\left(\bar{\mu}'\right) + \pi\,\left(n_{\downarrow}(\bar{S}) - n_{\uparrow}(\bar{S})\right)\,, \tag{A.9}$$

where $n_{\downarrow}(\bar{S})$ is the number of times μ' changes sign *from positive to negative* between 0 and $\bar{S}$, while $n_{\uparrow}(\bar{S})$ is the number of times μ' changes sign *from negative to positive*

$$n_{\downarrow}(\bar{S}) = 1 + \left\lfloor \frac{\bar{S}-1}{4} \right\rfloor\,, \tag{A.10}$$

$$n_{\uparrow}(\bar{S}) = 1 + \left\lfloor \frac{\bar{S}-3}{4} \right\rfloor\,, \tag{A.11}$$

where

$$\lfloor x \rfloor = x - \{x\}\,, \tag{A.12}$$

with $\{x\} = \mod(x,1)$ with mod being the module function.

The deformation is

$$\begin{aligned} x(\bar{S}) &= 1 - I_{c_\theta}\left(\bar{\mu}_1\right) + I_{c_\theta}\left(\bar{\mu}\right)\,,\\ y(\bar{S}) &= -I_{s_\theta}\left(\bar{\mu}_1\right) + I_{s_\theta}\left(\bar{\mu}\right)\,, \end{aligned} \tag{A.13}$$

with

$$I_{c_\theta} = \cos\beta_1\, I_{c_\beta}\left(\bar{\mu}\right) + \sin\beta_1\, I_{s_\beta}\left(\bar{\mu}\right)\,, \tag{A.14}$$

$$I_{s_\theta} = \sin\beta_1\, I_{c_\beta}\left(\bar{\mu}\right) - \cos\beta_1\, I_{s_\beta}\left(\bar{\mu}\right)\,, \tag{A.15}$$

and

$$I_{c_\beta} = \sqrt{\frac{2}{Q_0}}\,\bar{\mu}\,, \tag{A.16}$$

$$I_{s\beta} = \sqrt{\frac{2}{Q_0}}\,\left(\mathrm{sign}\left(\bar{\mu}'\right)\,I_2(S) + 2\,I_2(1)\,\left(n_{\downarrow}+n_{\uparrow}\right)\right)\,, \tag{A.17}$$

with

$$I_2(\bar{\mu}) = \int_0^{\bar{\mu}} \frac{\bar{\mu}^2}{\sqrt{1-\bar{\mu}^4}}\mathrm{d}\bar{\mu} = E(\arcsin\bar{\mu}\mid -1) - F(\arcsin\bar{\mu}\mid -1)\,, \tag{A.18}$$

where E is the *elliptic integral of the second kind* and F is the *elliptic integral of the first kind*.

The dimensionless strain energy functional is

$$U[Q_0] = \frac{1}{2}\int_0^1 \mu^2\,\mathrm{d}S\,, \tag{A.19}$$

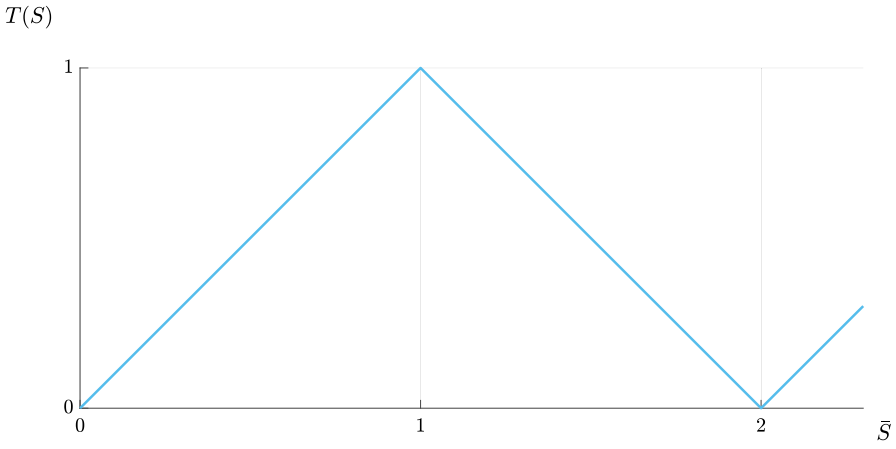

Fig. B.12. Level-set function for the solution in implicit form as in Eq. (B.4).

which can be computed to lead

$$U[Q_0] = \sqrt{2\,Q_0}\,\left(\text{sign}\left(\bar{\mu}_1'\right)\,I_2\left(\bar{\mu}_1\right) + 2\,I_2(1)\,\left(n_\downarrow + n_\uparrow\right)\right)\,, \tag{A.20}$$

with

$$\bar{\mu}_1 = \text{sn}\left(\frac{\sqrt{2\,Q_0}}{2}\,|-1\right)\,. \tag{A.21}$$

Appendix B. *Elastica* loaded by a uniform follower pressure: analytical solution

In this section, we use the solution derived in (Barbieri, 2020). For this case,

$$\mu_0' = 0\,,\qquad N_0 = 0\,,\qquad \mu_0 = M_0 = 0\,. \tag{B.1}$$

The Eq. (11) becomes

$$\mu'^2 + \frac{\mu^4}{4} - 2\,q\,\mu = 0\,. \tag{B.2}$$

The solution of Eq. (B.2) is also a periodic solution, with quarter-period $S_{\max}$, which, however, is always non-negative and oscillates between 0 and $\mu_{\max}$:

$$\mu_{\max} = 2\,q^{1/3}\,,\qquad S_{\max} = 2\,q^{-1/3}\,{}_2F_1\left(\frac{1}{6},\frac{1}{2};\frac{7}{6};1\right)\,, \tag{B.3}$$

where ${}_2F_1\left(\frac{1}{6},\frac{1}{2};\frac{7}{6};\cdot\right)$ is the *hypergeometric* function. The solution μ is given in implicit form:

$$I(\bar{\mu}) - T(\bar{S}) = 0\,, \tag{B.4}$$

with $T(\bar{S})$ being the level-set function showed in Fig. B.12. The role of T is to enforce the symmetry and the periodicity in the solution $\mu(S)$. Many expressions exist for the triangle wave in Fig. B.12: we suggest the following *surrogate* expression

$$T(\bar{S}) = \frac{2}{\pi}\,\arcsin\left(\,\left|\sin\left(\frac{\pi}{2}\,\bar{S}\right)\right|\,\right)\,, \tag{B.5}$$

and using the differentiation rule for implicit functions

$$\text{sign}\left(\mu'\right) = \text{sign}\left(\sin\left(\pi\,\bar{S}\right)\right)\,. \tag{B.6}$$

The function $I(\bar{\mu})$ is

$$I(\bar{\mu}) = \frac{\sqrt{\bar{\mu}}\;\;{}_2F_1\left(\frac{1}{6},\frac{1}{2};\frac{7}{6};\;\bar{\mu}^3\right)}{{}_2F_1\left(\frac{1}{6},\frac{1}{2};\frac{7}{6};1\right)}\,. \tag{B.7}$$

The variables $\bar{\mu}$ and $\bar{S}$ have the same meaning as in Eqs. (A.5). The rotation is given by Eq. (A.9) with

$$\beta(\bar{S}) = \frac{4}{3}\,\arcsin\bar{\mu}^{3/2}\,\text{sign}\,\bar{\mu}' + \frac{4}{3}\,\pi\,n_\downarrow(\bar{S})\,, \tag{B.8}$$

and the functions I_{c_β} and I_{s_β} for the deformation as in Eqs. (A.13) are

$$I_{c_\beta} = q^{-1/3}\left[C_c\,\mathbb{C}(\bar{\mu}) + S_c\,\mathbb{S}(\bar{\mu}) - \mathbb{C}(1)\,\sum\Delta C_c - \mathbb{S}(1)\,\sum\Delta S_c\right]\,, \tag{B.9}$$

$$I_{s_\beta} = q^{-1/3}\left[S_s\,\mathbb{C}(\bar{\mu}) - C_s\,\mathbb{S}(\bar{\mu}) - \mathbb{C}(1)\,\sum\Delta S_s + \mathbb{S}(1)\,\sum\Delta C_s\right]\,, \tag{B.10}$$

with the following being *piecewise constant* functions, with $\Delta\cdot$ denoting the amplitudes of the discontinuities at $\bar{\mu} = 1$:

$$\begin{aligned} C_c &= \cos\left(\tfrac{4}{3}\,\pi\,n_\downarrow\right)\,\text{sign}\,\bar{\mu}'\,,\\ S_c &= \sin\left(\tfrac{4}{3}\,\pi\,n_\downarrow\right)\,,\\ C_s &= \cos\left(\tfrac{4}{3}\,\pi\,n_\downarrow\right)\,,\\ S_s &= \sin\left(\tfrac{4}{3}\,\pi\,n_\downarrow\right)\,\text{sign}\,\bar{\mu}'\,, \end{aligned} \tag{B.11}$$

and

$$\begin{aligned} \mathbb{C}(\bar{\mu}) &= 2\,\sqrt{\bar{\mu}}\,\cos\left(\tfrac{4}{3}\,\arcsin\bar{\mu}^{3/2}\right)\,,\\ \mathbb{S}(\bar{\mu}) &= 2\,\sqrt{\bar{\mu}}\,\sin\left(\tfrac{4}{3}\,\arcsin\bar{\mu}^{3/2}\right)\,. \end{aligned} \tag{B.12}$$

The strain energy functional is given by

$$U[q] = 2\,q^{1/3}\,\left(\text{sign}\left(\bar{\mu}_1'\right)\,I_2\left(\bar{\mu}_1\right) + 2I_2(1)\,n_\downarrow\right)\,, \tag{B.13}$$

with

$$I_2\left(\bar{\mu}\right) = \frac{2}{5}\,\bar{\mu}_1^{5/2}\,{}_2F_1\left(\frac{1}{2},\frac{5}{6};\frac{11}{6};\kappa_1^3\right)\,. \tag{B.14}$$

Appendix C. Elastica loaded by a tangential follower force and an applied curvature: analytical solution

For this case,

$$\mu_0' = 0\,,\qquad N_0 > 0\,,\qquad \mu_0 = M_0 > 0\,,\qquad q = 0. \tag{C.1}$$

The Eq. (11) becomes

$$\mu'^2 = \frac{1}{4}\,\left(\mu^2 - {\mu_0}^2\right)\,\left({\mu_0}^2 + 4\,N_0 - \mu^2\right) \tag{C.2}$$

The solution of Eq. (C.2), for $N_0 > 0$, is a periodic function with quarter-period $S_{\max}$, always positive, with curvature oscillating between μ_0 and $\mu_{\max}$

$$\mu_{\max} = \sqrt{{\mu_0}^2 + 4\,N_0}\,,\qquad S_{\max} = \frac{1}{\mu_{\max}}\,K(1-m^2) \tag{C.3}$$

with K being the complete elliptic integral of the first kind, and $m = \mu_0/\mu_{\max}$.

Considering the boundary conditions $\mu(0) = \mu_0$ and $\mu'(0) = 0$, the complete solution is

$$\bar{\mu}(S) = \text{dn}\left(\frac{\mu_{\max}}{2}\,S - K(1-m^2)\,\middle|\,1-m^2\right) \tag{C.4}$$

where $\bar{\mu} = \mu/\mu_{\max}$, with K being the complete elliptic integral of the first kind, and F being the incomplete elliptic integral of the first kind and $\mathrm{dn}(x\,|k)$ is the Jacobi dn function of modulus k. For the cases of our interest ($\mu_0 \approx 0$ and $N_0 \gg 1$), $S_{\max} > 1$, therefore the rotation is

$$\theta(S) = \beta_1 - \beta(S) \qquad \beta_1 = \beta(1) \qquad \beta = \pi - 2\arctan\left(\frac{\sqrt{1-\bar{\mu}^2}}{\sqrt{\bar{\mu}^2 - m^2}}\right) \tag{C.5}$$

If θ_0 and N_0 are fixed, then the tip curvature μ_0 can be obtained by solving a nonlinear equation:

$$\beta_1(\mu_0, N_0) = \theta_0 \tag{C.6}$$

For the deformation, the functions I_{c_β} and I_{s_β} for the deformation as in Eqs. (A.13) are

$$I_{c_\beta} = \frac{2}{\mu_{\max}}\left(\frac{\mathrm{F}\left(\mathrm{asin}\,(\bar{\mu})\left|\frac{1}{m^2}\right.\right)\,1\mathrm{i} - \frac{m^2\,\mathrm{E}\left(\mathrm{asin}(\bar{\mu})\left|\frac{1}{m^2}\right.\right)2\mathrm{i}}{m^2-1}}{m} - \frac{\mathrm{F}\left(\mathrm{asin}\,(m)\left|\frac{1}{m^2}\right.\right)\,1\mathrm{i} - \frac{m^2\,\mathrm{E}\left(\mathrm{asin}(m)\left|\frac{1}{m^2}\right.\right)2\mathrm{i}}{m^2-1}}{m}\right) \tag{C.7}$$

$$I_{s_\beta} = \frac{4}{\mu_{\max}}\,\frac{1}{1-m^2}\,(\bar{\mu} - m) \tag{C.8}$$

with $1\mathrm{i} = \sqrt{-1}$. The strain energy functional is

$$U[N_0] = \mu_{\max}\, I_U(\bar{\mu}_1) \tag{C.9}$$

with $\bar{\mu}_1 = \bar{\mu}(1)$ (scaled curvature at the root of the cantilever) and

$$I_U = 1\mathrm{i}\,m\left[F\left(\arcsin\bar{\kappa}_1\left|\frac{1}{m^2}\right.\right) - E\left(\arcsin\bar{\kappa}_1\left|\frac{1}{m^2}\right.\right)\right] - 1\mathrm{i}\,m\left[F\left(\arcsin m\left|\frac{1}{m^2}\right.\right) - E\left(\arcsin m\left|\frac{1}{m^2}\right.\right)\right] \tag{C.10}$$

References

Anderson, T.L., 1991. Fracture Mechanics: Fundamentals and Applications. CRC Press.

Antman, S., 1968. General solutions for plane extensible elasticae having nonlinear stress-strain laws. Quart. Appl. Math. 26 (1), 35–47.

Antman, S.S., 1995. Nonlinear Problems of Elasticity. Springer.

Aoi, S., Egi, Y., Tsuchiya, K., 2013. Instability-based mechanism for body undulations in centipede locomotion. Phys. Rev. E 87 (1), 012717.

Barbieri, E., 2020. Analytical solution of the cantilevered elastica subjected to a normal, uniformly distributed follower load. Int. J. Solids Struct.

Bayly, P., Dutcher, S., 2016. Steady dynein forces induce flutter instability and propagating waves in mathematical models of flagella. J. R. Soc. Interface 13 (123), 20160523.

Berry, M., Shukla, P., 2015. Hamiltonian curl forces. Proc. R. Soc. A 471 (2176), 20150002.

Berry, M., Shukla, P., 2016. Curl force dynamics: symmetries, chaos and constants of motion. New J. Phys. 18 (6), 063018.

Bigoni, D., 2012. Nonlinear Solid Mechanics: Bifurcation Theory and Material Instability. Cambridge University Press.

Bigoni, D., Kirillov, O.N., Misseroni, D., Noselli, G., Tommasini, M., 2018a. Flutter and divergence instability in the Pflüger column: Experimental evidence of the Ziegler destabilization paradox. J. Mech. Phys. Solids 116, 99–116.

Bigoni, D., Misseroni, D., 2020. Structures loaded with a force acting along a fixed straight line, or the "reut's column problem". J. Mech. Phys. Solids 134, 103741.

Bigoni, D., Misseroni, D., Tommasini, M., Kirillov, O.N., Noselli, G., 2018b. Detecting singular weak-dissipation limit for flutter onset in reversible systems. Phys. Rev. E 97 (2), 023003.

Bigoni, D., Noselli, G., 2011. Experimental evidence of flutter and divergence instabilities induced by dry friction. J. Mech. Phys. Solids 59 (10), 2208–2226.

Botto, L., 2019. Towards nanomechanical models of liquid-phase exfoliation of layered 2d nanomaterials: analysis of a pi-peel model. Front. Mater. 6, 302.

De Canio, G., Lauga, E., Goldstein, R.E., 2017. Spontaneous oscillations of elastic filaments induced by molecular motors. J. R. Soc. Interface 14 (136), 20170491.

Frisch-Fay, R., 1962. Flexible Bars. Butterworths.

Gravelle, S., Kamal, C., Botto, L., 2020. Liquid exfoliation of multilayer graphene in sheared solvents: a molecular dynamics investigation. The Journal of Chemical Physics 152 (10), 104701.

Hodges, S., Jensen, O., 2002. Spreading and peeling dynamics in a model of cell adhesion. J. Fluid Mech. 460, 381.

Kendall, K., 1971. The adhesion and surface energy of elastic solids. J. Phys. D: Appl. Phys. 4 (8), 1186.

Kendall, K., 1975. Thin-film peeling-the elastic term. J. Phys. D: Appl. Phys. 8 (13), 1449.

Kirillov, O.N., 2013. Nonconservative Stability Problems of Modern Physics, Vol. 14. Walter de Gruyter.

Lenoach, B., 1995. The crack tip solution for hydraulic fracturing in a permeable solid. J. Mech. Phys. Solids 43 (7), 1025–1043.

Libai, A., Simmonds, J.G., 1988. The Nonlinear Theory of Elastic Shells, One Spatial Dimension. Academic Press.

Lindahl, N., Midtvedt, D., Svensson, J., Nerushev, O.A., Lindvall, N., Isacsson, A., Campbell, E.E., 2012. Determination of the bending rigidity of graphene via electrostatic actuation of buckled membranes. Nano Lett. 12 (7), 3526–3531.

Mandre, S., Mahadevan, L., 2009. A generalized theory of viscous and inviscid flutter. Proc. R. Soc. A 466 (2113), 141–156.

Medvedovski, E., Roghanizad, M., Leal Mendoza, G., Cai, W., Hendricks, R.W., 2020. Influence of iron boride coating on flow-accelerated corrosion of carbon steel. Adv. Eng. Mater. 2000354.

Misseroni, D., Barbieri, E., Pugno, N.M., 2021. Extreme deformations of the cantilever Euler Elastica under transverse aerodynamic load. Extreme Mech. Lett. 42, 101110.

Paton, K.R., Varrla, E., Backes, C., Smith, R.J., Khan, U., O'Neill, A., Boland, C., Lotya, M., Istrate, O.M., King, P., et al., 2014. Scalable production of large quantities of defect-free few-layer graphene by shear exfoliation in liquids. Nat. Mater. 13 (6), 624–630.

Pigolotti, L., Mannini, C., Bartoli, G., Thiele, K., 2017. Critical and post-critical behaviour of two-degree-of-freedom flutter-based generators. J. Sound Vib. 404, 116–140.

Rivlin, R.S., 1944. The effective work of adhesion. Paint Technol. 9 (106), 215.

Rohde, F., 1953. Large deflections of a cantilever beam with uniformly distributed load. Quart. Appl. Math. 11 (3), 337–338.

Roman, B., 2013. Fracture path in brittle thin sheets: a unifying review on tearing. Int. J. Fract. 182 (2), 209–237.

Salussolia, G., Barbieri, E., Pugno, N.M., Botto, L., 2020. Micromechanics of liquid-phase exfoliation of a layered 2D material: A hydrodynamic peeling model. J. Mech. Phys. Solids 134, 103764.

Shampine, L.F., 2008. Vectorized adaptive quadrature in MATLAB. J. Comput. Appl. Math. 211 (2), 131–140.

Sugiyama, Y., Katayama, K., Kinoi, S., 1995. Flutter of cantilevered column under rocket thrust. J. Aerosp. Eng. 8 (1), 9–15.

Sugiyama, Y., Katayama, K., Kiriyama, K., Ryu, B.-J., 2000. Experimental verification of dynamic stability of vertical cantilevered columns subjected to a sub-tangential force. J. Sound Vib. 236 (2), 193–207.

Sugiyama, Y., Langthjem, M., Ryu, B., 1999. Realistic follower forces. J. Sound Vib. 225 (4), 779–782.

Tommasini, M., Kirillov, O.N., Misseroni, D., Bigoni, D., 2016. The destabilizing effect of external damping: Singular flutter boundary for the Pflüger column with vanishing external dissipation. J. Mech. Phys. Solids 91, 204–215.

Wood, W., Saw, S., Saunders, P., 1969. The kinetic stability of a tangentially loaded strut. Proc. R. Soc. A 313 (1513), 239–248.

Zehnder, A.T., Potdar, Y.K., 1998. Williams meets von Karman: Mode coupling and nonlinearity in the fracture of thin plates. Int. J. Fract. 93 (1-4), 409.